1D-2D-3D Transformation Synthesis of Hierarchical Metal-Organic Framework Adsorbent for Multicomponent Alkane Separation

Wee, Lik H.; Meledina, Maria; Turner, Stuart; Van Tendeloo, Gustaaf; Zhang, Kang; Rodriguez-Albelo, Marleny L.; Masala, Alessio; Bordiga, Silvia; Jiang, Jianwen; Navarro, Jorge A. R.; Kirschhock, Christine E. A.; Martens, Johan A.. 1D-2D-3D Transformation Synthesis of Hierarchical Metal-Organic Framework Adsorbent for Multicomponent Alkane Separation. JOURNAL OF THE AMERICAN CHEMICAL SOCIETY. 139 (2) pp: 819-828.
DOI: 10.1021/jacs.6b10768

1D-2D-3D Transformation Synthesis of Hierarchical Metal-Organic Framework Adsorbent for Multicomponent Alkane Separation

Lik H. Wee[†*], Maria Meledina[‡], Stuart Turner[‡], Gustaaf Van Tendeloo[‡], Kang Zhang[#], L. Marleny Rodriguez-Albelo[‖], Alessio Masala[⊥], Silvia Bordiga[⊥], Jianwen Jiang[#*], Jorge A. R. Navarro[‖*], Christine E. A. Kirschhock[†*] and Johan A. Martens[†]

[†]Centre for Surface Chemistry and Catalysis, University of Leuven, Celestijnenlaan 200f, B3001, Heverlee, Leuven, Belgium.

[‡]Electron Microscopy for Materials Science, University of Antwerp, Groenenborgerlaan 171, B2020, Antwerp, Belgium.

[#]Department of Chemical and Biomolecular Engineering, National University of Singapore, 117576, Singapore.

[‖]Departamento de Química Inorgánica, Universidad de Granada, Av. Fuentenueva S/N, 18071 Granada, Spain.

[⊥]Department of Chemistry, NIS and INSTM Centre of Reference, University of Turin, Via Quarello 15, I-10135, Torino, Italy.

KEYWORDS: Copper benzenetricarboxylate metal-organic framework, hierarchical, alkane separation, solid-solid phase transformation

ABSTRACT: A new hierarchical MOF consisting of Cu(II) centers connected by benzene-tricarboxylates (BTC) is prepared by thermo-induced solid transformation of a dense CuBTC precursor phase. The mechanism of the material formation has been thoroughly elucidated and revealed a transformation of a ribbon-like 1D building unit into 2D layers and finally a 3D network. The new phase contains excess copper, charge compensated by systematic hydroxyl groups, which leads to an open microporous framework with tunable permanent mesoporosity. The new phase is particularly attractive for molecular separation. Energy consumption of adsorptive separation processes can be lowered by using adsorbents that discriminate molecules based on adsorption entropy rather than enthalpy differences. In separation of a 11-component mixture of C_1-C_6 alkanes, the hierarchical phase outperforms the structurally related microporous HKUST-1 as well as silicate-based hierarchical materials. Grand canonical Monte Carlo (GCMC) simulation provides microscopic insight into the structural host-guest interaction confirming low adsorption enthalpies and significant entropic contributions to the molecular separation. The unique three-dimensional hierarchical structure as well as the systematic presence of Cu(II) unsaturated coordination sites cause this exceptional behavior.

INTRODUCTION

The supramolecular coordination bonding between transition-metal cations and multidentate organic linkers has given rise to a relatively new class of porous hybrid material known as metal-organic frameworks (MOFs).[1-7] MOFs offer exceptional internal surface area, tunable pore architectures and high chemical functionalities suited for a vast range of promising applications ranging from catalysis,[8,9] gas storage,[10-13] separation,[14] chemical sensing[15] to bio-imaging and drug delivery.[16] Over the last two decades, the versatility of MOFs based on the large choice of inorganic and organic components has resulted in more than 20,000 MOFs with unique topologies.[5] Optimization of MOFs for fine chemical transformation and separation processes depends on avoidance of too confining pore systems, hindering molecular diffusion and mass transfer, especially when large molecules are involved.[17,18] The synthesis of hierarchical MOFs possessing intrinsic micropores in addition to secondary meso- or even macropore therefore is of high interest. Various methods such as secondary building units,[19] extended-linkers,[20-22] mixed-linkers,[23,24] surfactant-templated synthesis,[25,26] acid leaching[27] and modulated synthesis[28,29] have been reported as possible routes towards hierarchical MOFs, but the number of stable mesoporous MOFs is relatively small (< 1%). In most cases pore systems of MOFs are restricted to the microporous regime, mainly due to framework instability and interpenetration.[30,31]

Improving efficiency of molecular separation processes can result in significant energy savings in chemical industry. Production of high-grade gasoline is a prominent example. In this fuel, alkanes are preferred over aromatics for environmental reasons. Gasoline with high research octane number (RON) of 95, 98 and 100 is en-

riched with 2,3-dimethylbutane (RON = 105) and 2,2-dimethylbutane (RON = 94) at the expense of less valuable monobranched isomers such as 2-methylpentane (RON = 74), 3-methylpentane (RON = 75) and linear *n*-hexane (RON = 30).[32] In industrial gasoline manufacturing, low RON molecules are recycled to an isomerization reactor to branch their carbon skeleton. In this application separation by fractional distillation is prohibitively expensive. Using adsorption technology, manufacturing high octane gasoline critically depends on the adsorbents' capability of sorting molecules according to their octane number. Currently, zeolite 5A is used to separate normal from branched alkanes. Adding zeolite beta to separate mono- from di-branched hexane isomers partially improves the process,[33-35] but there remains ample room for further improvement. Especially the separation of mono- from di-branched C_6 isomers with the highest octane number remains a challenge.

Molecular sieving is an ideal option if sufficient difference in diffusivity is coupled to selective exclusion of the bulkiest compounds from the pores. An alternative option is to strive for high selectivity at adsorption equilibrium, exploiting packing effects in entropy driven separation, or preferential interaction of specific compounds from the mixture with pore walls in enthalpy driven systems. The desired separation of C_6 gasoline compounds involves the use of narrow pores hardly wider than the molecules and is leading to strong physisorption. Too strong adsorption obviously leads to the need of heating to higher temperatures to desorb and displace the molecules from the adsorbent's pores.[36]

Reducing the adsorption enthalpy while maintaining the entropic contribution to the adsorption equilibrium could in principle lead to separation at lower temperatures, which would reduce energy consumption. The enthalpy of adsorption of hydrocarbons is dominated by van der Waals interaction, increasing with polarizability, which increases with atomic weight.[36] As expected from the lower atomic weight of the C, H, and N elements typically composing the organic linkers, adsorption enthalpies on MOFs are generally lower compared to zeolites consisting of heavier silicon and aluminum atoms bonded with oxygen. On zeolite beta, the heat of adsorption of hexane isomers is significant ($-\Delta H > 65$ kJ mol^{-1}) and separation is achieved at temperatures between 423 and 523 K, substantially above the boiling point range of 323-333 K.[37] Several MOFs have been demonstrated as capable of separating mixture of hydrocarbons.[37-48] Literature data on the use of MOFs for adsorptive separation of C_6 hydrocarbon mixtures confirm the enthalpy bonus of the organic pore walls.[37]

In this work, a new hierarchical copper benzentricarboxylate COK-18 (COK-18 = Centrum voor Oppervlaktechemie en Katalyse No. 18) MOF was synthesized via thermo-induced 1D-2D-3D transformation. It is demonstrated the implementation of a 3D interconnected hierarchical pore system allows maximizing entropy differences, while minimizing transport limitation during multicomponent hydrocarbon separation at low temperature.

RESULTS AND DISCUSSION

Synthesis and characterization of COK-18. COK-18 is a novel hierarchical MOF consisting of Cu(II) centers connected by benzene-tricarboxylates (BTC). Compared to conventional microporous HKUST-1, COK-18 contains excess copper, charge compensated by systematic hydroxyl groups, which leads to an open microporous framework with tunable mesoporosity. COK-18 is synthesized via thermo-induced solid-solid transformation of a dense crystalline CuBTC precursor. The precursor can easily be prepared by room temperature precipitation of copper nitrate trihydrate and BTC in a water/ethanol solution. The crystalline light blue precipitate was identified as phase pure catena (Triaqua-(\m~2~-1,3,5-benzenetricarboxylate-O,O')-copper(ii)) referred to as H1 phase by Pech and Pickardt.[49] 48h thermal treatment of this precursor in its supernatant containing solvated Cu^{2+} ions resulted in a dark blue new phase [COK-18; $Cu_{20}(C_9H_3O_6)_8(OH)_{16}] \cdot x H_2O$ with a high synthesis yield of >95% based on Cu.

Striated patterns on the crystal surfaces hallmark the spongy morphology of COK-18 (Figure 1a). The porosity of COK-18 is confirmed by nitrogen physisorption in comparison to HKUST-1 (Figure 1b,d). The nitrogen adsorption-desorption isotherm of COK-18 (Figure 1b) exhibits Type I behavior confirming the presence of micropores and a hysteresis loop ascribed to mesoporosity.[50,51] The Brunauer-Emmet-Teller (BET) and Langmuir surface areas are 800 and 1098 m^2 g^{-1}, respectively. The calculated total pore volume is 0.45 cm^3 g^{-1} with a mesopore volume of 0.07 cm^3 g^{-1}. The hierarchical pore architecture of COK-18 is verified by Density Functional Theory (DFT) and Barrett-Joyner-Halenda (BJH) methods revealing a micropore size of 1.1 nm in addition to textural mesoporosity with an average pore diameter of 12 nm (Figure 1b, insert and Figure S1). The corresponding Type H4 hysteresis suggests that the largest mesopores are of slit-like shape, as confirmed by TEM.[50,51]

A combination of bright field transmission electron microscopy (BF TEM), selected area electron diffraction (SAED), high angle annular dark field scanning transmission electron microscopy (HAADF-STEM) and electron tomography was used to investigate the morphology and structure of the COK-18 particles. BF TEM imaging (Figure 1e) clearly demonstrates the presence of elongated bright contrast features corresponding to the slit-like pores evenly distributed around the COK-18 particle. SAED (Figure 1f) confirms the crystallinity of the new material and lowering of the symmetry from the *Fm-3m* space group for the HKUST-1 material to *Immm* for the new COK-18 structure as evidenced also from the Rietveld refinement of the XRD data (*vide infra*).[52] However, as EM images only provide 2D information of the 3D object, we used electron tomography to investigate the location of the pores throughout the COK-18 particles.

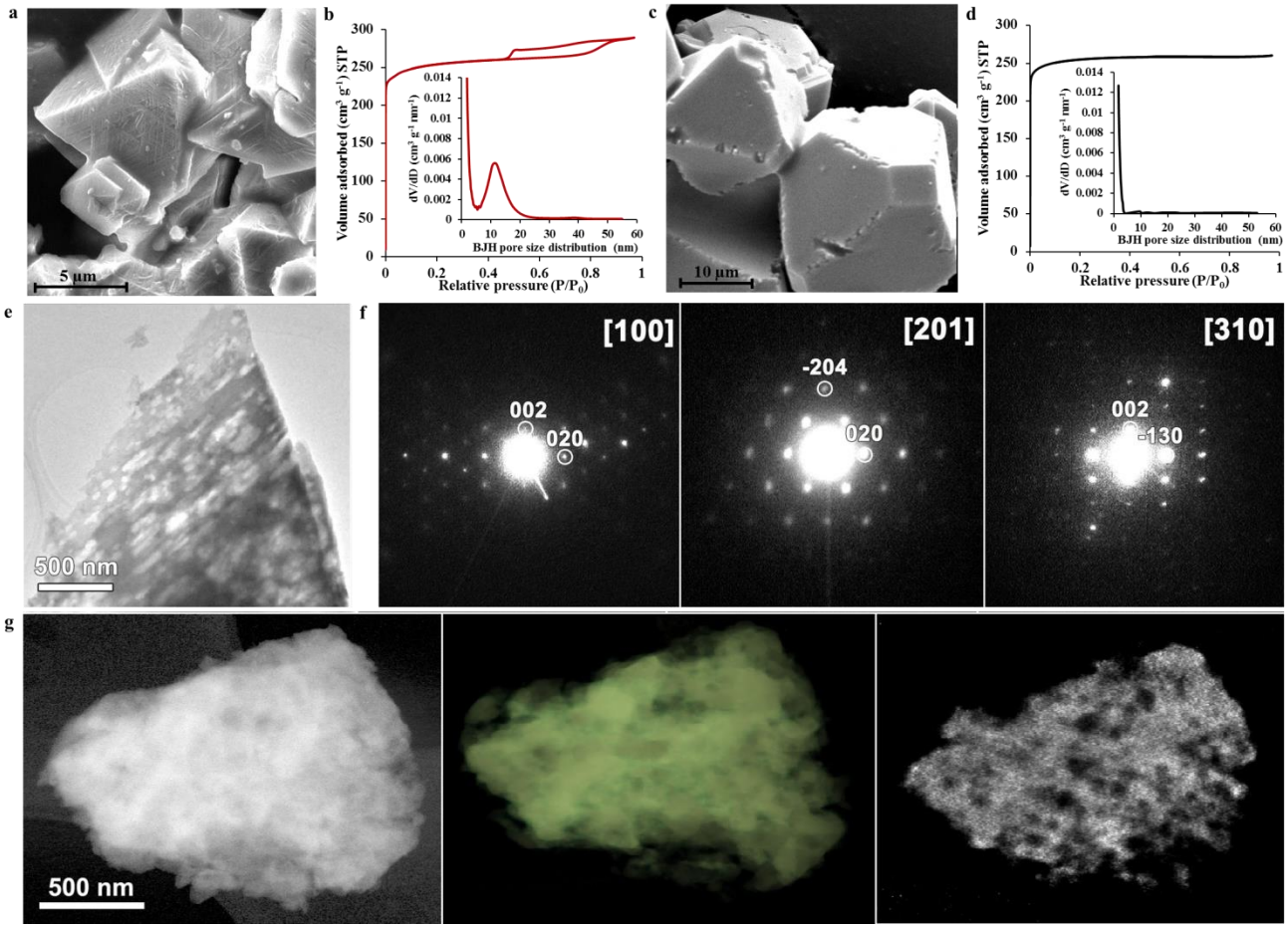

Figure 1. SEM images of (a) COK-18 and (c) HKUST-1. N_2 adsorption-desorption isotherms of (b) COK-18 and (d) HKUST-1. The inserts show the corresponding BJH pore size distributions. (e) BF TEM image showing a COK-18 particle. (f) SAED patterns of the COK-18 material recorded along the [100], [201] and [310] zone axis. (g) HAADF-STEM image of a COK-18 particle used to record the tomographic tilt series together with the reconstruction of the volume and an orthoslice through the reconstructed volume.

Figure 1g shows a COK-18 particle ~ 1,5 µm in size, used to acquire the tilt series together with the reconstructed volume and an orthoslice through the particle. It is clearly visible that the pores are inside the COK-18 particle creating a "Swiss cheese" morphology (see Movie S1).

According to TG analysis (Figure S2), COK-18 has a similar thermal stability (up to 513 K) as HKUST-1. Upon evacuation at 453 K in a dynamic vacuum, both HKUST-1 and COK-18 change color from cyan to navy blue. Such darkening indicates a change in the coordination of copper, owing to chemisorbed water. The physical and structural characteristics of COK-18 were studied by FTIR (Figure 2). Peculiar to COK-18, is the presence of a sharp band at 821 cm^{-1}, assigned to a bending mode of hydroxyl groups, which persists after outgassing (Figure 2a). Differences between H1 and COK-18 are even more pronounced in spectra collected in ATR mode (Figure S3). In far-IR (Figure 2a, insert), COK-18 and HKUST-1 show similar Cu-O modes as evidenced by a main band at 492 cm^{-1} and a shoulder at 476 cm^{-1}, in addition to Cu-Cu modes at lower frequencies (320, 266 and 222 cm^{-1}), which confirms the presence of Cu-pairs.[53]

The Cu-environment of the two materials was studied by IR spectroscopy using CO as probe molecule at 100 K (Figure 2b). Though of similar nature, interaction sites for CO are more abundant in COK-18 and desorption is faster upon degassing. At higher coverage by CO three main components are observed (2172, 2141 and 2128 cm^{-1}). The sharp band at 2179–2170 cm^{-1} is ascribed to the formation of reversible Cu^{2+}....CO adducts,[53] an interesting feature which has been also been observed at low CO coverage of Cu^{2+} exchanged zeolites.[54] The red shift of this band with increasing coverage indicates conversion of monocarbonyls into dicarbonyls without splitting of the C–O modes into symmetric and antisymmetric stretching modes. The high intensity of this signal in COK-18 demonstrates that the adsorption of two CO molecules on one Cu-site occurs much more often compared to HKUST-1, where such an arrangement is only possible at defects or at the crystal surface. Satellites of the main peaks at 2191 and 2148 cm^{-1} are attributed to asymmetric and symmetric stretching

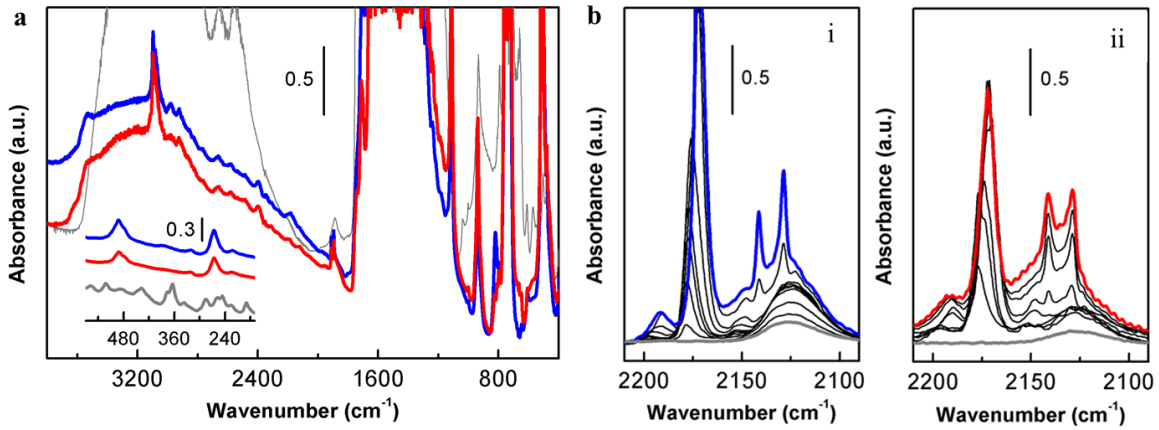

Figure 2. (a) Mid-IR spectra of activated COK-18 (blue curve), HKUST-1 (red curve) and H1 phase (grey curve). Far-IR spectra of the three samples in air (diluted in paraffin) are presented in the inset with the same colour code. (b) FTIR spectra in the increasing coverages of CO on (i) COK-18 and (ii) HKUST-1. All samples were activated under vacuum conditions at 453 K for 2 hours. FTIR spectra relative to CO adsorption were recorded at 77 K.

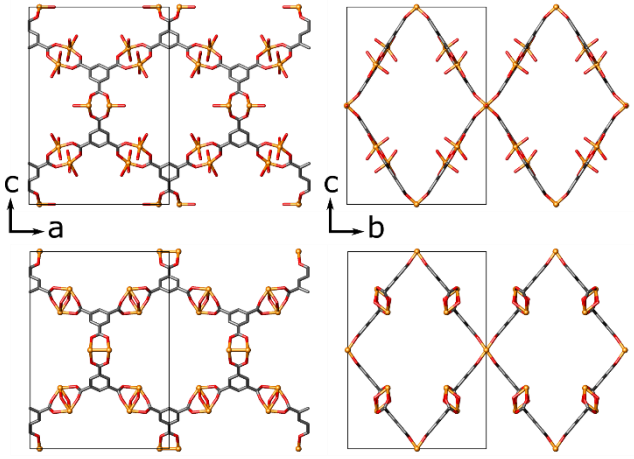

Figure 3. Crystal structure of COK-18. As made material (top) and COK-18 activated at 443 K (bottom).

modes of Cu^{2+}....(CO)2.[55] Two sharp peaks observed at 2141 and 2128 cm^{-1} with high reversibility are assigned to CO hindered by BTC linkers in its vicinity.[56] It should be noted that this hindrance is more pronounced in HKUST-1 compared to COK-18.

COK-18 shows high Bragg crystallinity and the X-ray diffraction pattern resembles that of HKUST-1. However, COK-18 adopts the orthorhombic space group *Immm* instead of the cubic space group *Fm-3m*.[50] This deviation from cubic symmetry was also confirmed by TEM. The structural parameters of HKUST-1, transformed to *Immm,* described the COK-18 pattern well, except that Rietveld refinement systematically indicated systematically missing BTC. The structure of HKUST-1 is assembled by hexagonal layers of BTC connected by Cu(II) pairs. These layers intersect to form the typical paddlewheel motif. Reducing the symmetry to *Immm* removes the equivalence between these (111) planes resulting in 2 sets of planes rotated by 90°. Removal of one set of these allowed excellent description of the observed powder diffraction data. This model also explains the peculiar porosity as well as the presence of hydroxyls and the increased number of unpaired Cu^{2+} species. The arrangement of the hexagonal layers leads to rhombic pores and an open pore structure, as well as incomplete paddlewheels. Here a copper-pair connects only 2 linkers in a plane and completes coordination with 2 hydroxyls and water as shown in Figure 3 (top). Analysis of the occupation numbers of these planar motifs indicated that about 50% of the BTC linkers are connected only by one single copper ion. Rietveld refinement of activated COK-18 reveals the same topology but here the carboxy-functions in incomplete paddlewheels are turned out of plane of the aromatic rings as presented in Figure 3 (bottom). The associated copper dimers in the system still contain two extra ligands, which are assigned as hydroxyls, based on FTIR.

1D-2D-3D solid-solid phase transformation. The underlying thermo-induced phase transformation mechanism of the dense precursor phase into COK-18 was studied by scanning electron microscopy (SEM), N_2 physisorption and powder X-ray diffraction (PXRD) (Figure 4). H1 precursor and the products collected at different solvothermal treatment times (3, 6, 9, and 12h) show significant changes in morphology (Figure 4c). The dense precursor phase appears as elongated slabs (10-20 µm) with smooth surfaces. No porosity was noted according to N_2 physisorption (Figure 4d). After 3h these slabs appear to have swollen and show laminar features. Already at this stage significant microporosity next to mesoporosity has evolved (Figure 4d and Table S1). After 6h, the material appears flaky, without expressed facets, which emerge more clearly after 9h, where the layers seem to have aligned. During this time no changes of microporosity but a substantial increase of mesoporosity is observed. After 12h the spongy octahedra, typical for COK-18 are discernible and the microporosity has strongly increased (Figure 4d and Table S1).

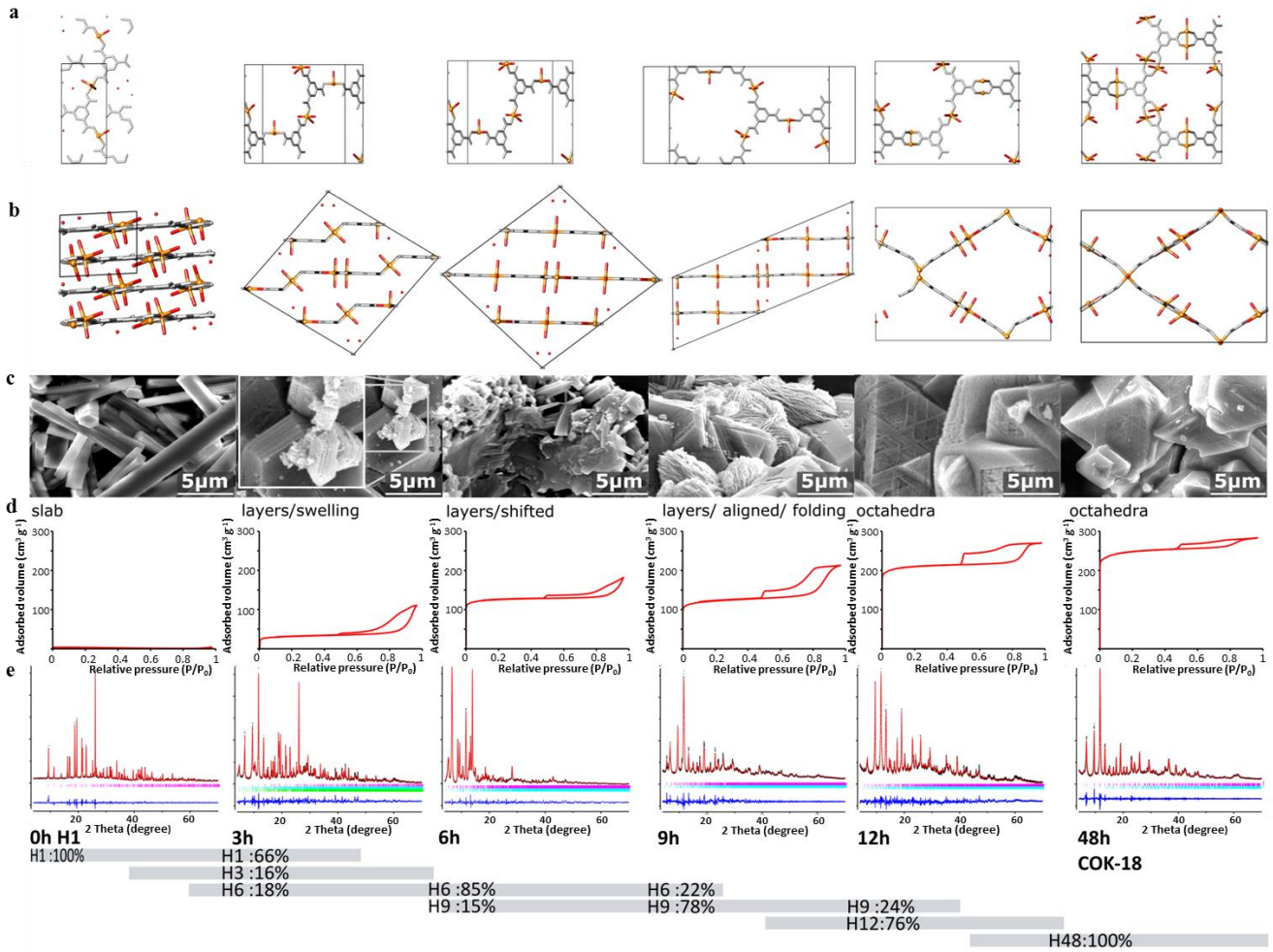

Figure 4. Crystal structures with (a) top and (b) side view of the Cu-BTC ribbons. (c) SEM images, (d) nitrogen physisorption isotherms, (d) Rietveld refinements and phase composition at different synthesis times of 0, 3, 6, 9, 12,and 48 hours (from left to right). H1= dense crystalline CuBTC precursor phase, H3= CuBTC intermediate phase obtained after 3h, H6= CuBTC intermediate phase obtained after 6h, H9= CuBTC intermediate phase obtained after 9h, H12= CuBTC intermediate phase obtained after 12h, and H48= COK-18 obtained after 48h.

The rapid structural transformation as well as the observed textural changes indicate a solid-solid transformation (Figure 4). Throughout the transformation process the solid shows high Bragg crystallinity, with a number of reflections persisting from the H1 phase till the final COK-18 (Figure 4e, Table S2-S7 and Figure S4-S8). This implies that at least some structural features and dimensions are preserved. The H1 phase consists of planar zig-zag ribbons of BTC molecules linked by single Cu(II) ions. These 1D ribbons translate sideways, where the third, still protonated carboxyl function of each linker hydrogen-bonds to the adjacent zig-zag chain (Figure 4a,b). The resulting layers are stacked in overall monoclinic symmetry. Interestingly, the arrangement of copper and BTC within the ribbons already is part of the coordinatively bound hexagonal layers observed in COK-18. Indeed, the repetition value along the ribbons of roughly 18.8 Å is the length preserved throughout the transformation. With this information an assignment of the reflections at the various stages of transformation was attempted. It was assumed that on average the transformation occurs gradually so that at each time more than one phase is present and that states close in time contain the same or at least similar phases. Based on the symmetry of the ribbons containing a twofold screw axis the diffraction patterns were analyzed for the presence of one or more phases with the minimum space group $P2_1$, and *b*-axis around 18.5 Å. 3 distinct phases were identified by recursive indexing between the precursor phase H1 and COK-18, which already was present after 12h (Figure 4e and Table S8). The obtained unit cells were analyzed for their content based on the assumption that the ribbon units are present throughout. The resulting models were used for Rietveld refinements resulting in good agreement with the experimental data (Figure 4e). An elegant scenario unfolds upon study of the structures. After 3h still some H1 precursor persists, but most ribbons have tilted along their axis forming undulating hexagonal

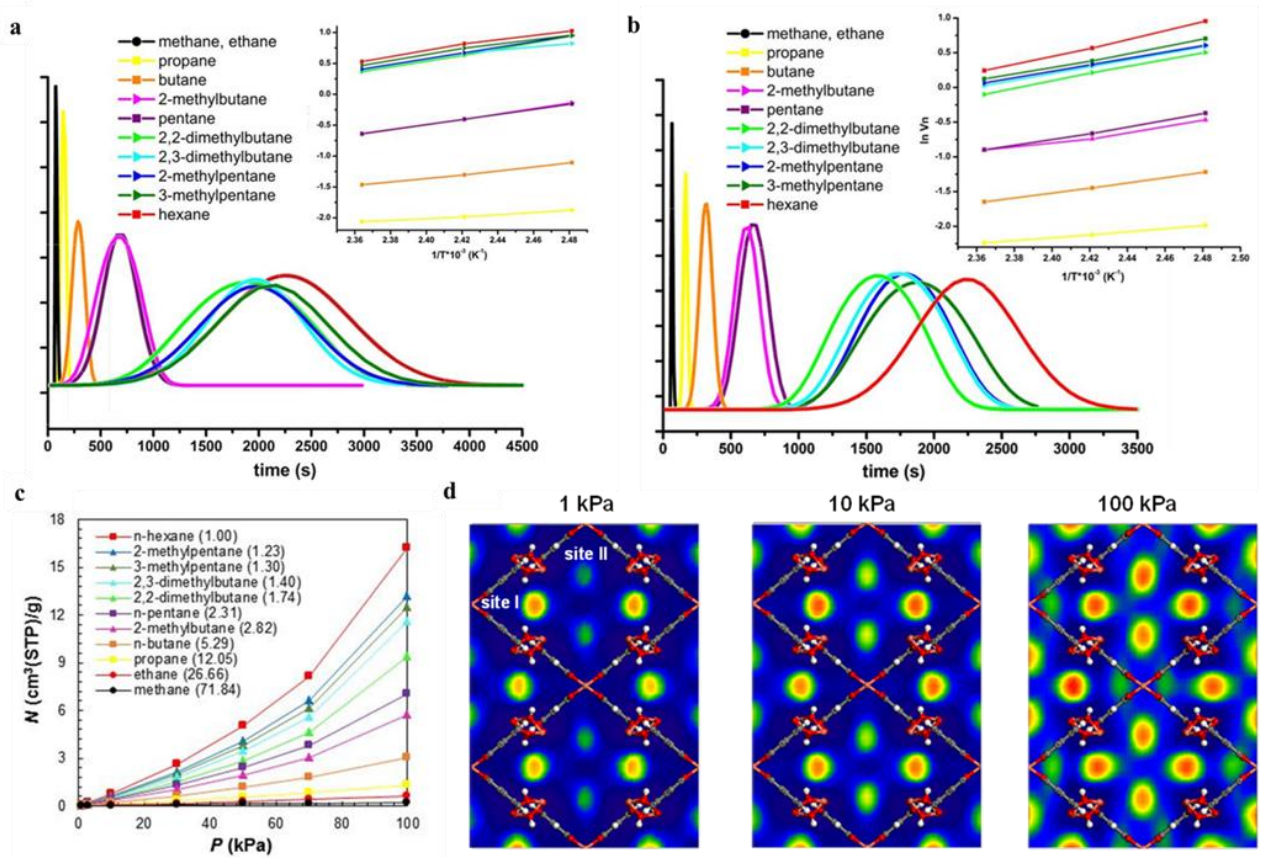

Figure 5. Pulse gas chromatogram of a gas mixture of C_1-C_6 alkanes on (a) HKUST-1 and (b) COK-18 at 423 K. The inset shows the respective van't Hoff plots for the investigated adsorbents. (c) Simulated adsorption isotherms of 11-component mixture in COK-18 at 373 K. The legend follows the order of adsorption capacity. The values in the parentheses denote the partition coefficients $\alpha_{hexane/X}$ at 1 bar. (d) Density distribution contours of *n*-hexane in COK-18 at 373 K obtained from GCMC. The unit of density scale is the number of molecules per Å^3.

sheets (Figure 4a,b). Next to this 3h structure, another structure after 6h is present. Here the 2-dimensional hexagonal sheets are flattened. Though the presence of 3 phases, makes the direct analysis of the observed electron density ambiguous, the presence of Cu(II) between carboxyl functions of newly connected ribbons was derived. This Cu(II) presumably diffused into the solid precursor from the supernatant, which also is confirmed by the change of its color from blue to colorless. It stands to reason that these copper ions preferentially interact with those carboxy-functions in H1, which are not yet coordinated to Cu^{2+}. This leads to the connection of ribbons in neighboring layers, first forming undulating sheets which are then flattened (Figure 4c and Figure S9). The resulting swelling behavior is also observed from the SEM images (Figure 4c) supported by the significantly increased porosity (Figure 4d). After 6 hours, the 6h phase is dominant and no evidence for H1 or 3h structure remains. However a third phase has emerged where the flat hexagonal layers have realigned to congruence (9h). This change is in accordance with the flaky appearance in SEM and almost unchanged microporosity, but with a significant increase in mesoporosity (Figure 4c,d). The same two phases are still present after 9h in reversed amounts. Most of the layers are now fully aligned. After 12h the microporosity has almost doubled and octahedra, reminiscent of COK-18, are present (Figure 4d). In this sample still about 25% of 9h phase persists (Figure 4e and Table S8). In the rest the hexagonal layers have folded zig-zag wise to connect and finally form the paddlewheels between them. Though this 12h structure is still distorted it already shows the same 3D connectivity as observed in COK-18. The transformation scheme and the folding mechanism of the nano-ribbons into octahedra are illustrated in Movie S2 and Movie S3, respectively. In comparison to the recently reported mechanochemical solid state synthesis of a new *katsenite* topology by Friščić and coworkers,[57] our thermo-induced solid state synthesis demonstrates the transformation of a 2D non-porous CuBTC layered material to a 3D hierarchical COK-18, whereas the mechano-chemical synthesis method shows transformation of ZIF-8 to an amorphous intermediate before expression of the final structure *katsenite*-Zn(Methylimidazole)2, which consists of small channels and pockets resulting in a low BET surface area of 37 m^2 g^{-1}.[57] In the case of COK-18 the intermediate phases

are crystalline throughout and preservation of the original ribbon-like building unit is demonstrated for each time. In previous work, mesostructures could also be generated through stacking of $Cu_3(BTC)_2$ HKUST-1 nanoparticles, as demonstrated by Peng *et al.*[28] and Cao *et al.*[29] involving downsizing of particle size accomplished by CO_2 and acetic acid modulation, respectively. In those approaches, the original structure of the HKUST-1 material is preserved. In contrast, our solid-solid transformation synthesis approach gives rise to a new COK-18 topology possessing both the micro- and mesopores in a continuous phase.

Multicomponent alkane mixture separation. Pulse gas chromatography experiments were performed in the temperature range 403-433 K, using a complex gas mixture containing eleven C_1-C_6 alkanes (see Methods). HKUST-1 and COK-18 column packings were compared. The alkanes elute from the columns in the order of increasing carbon number (Figure 5a,b). On HKUST-1 isomers in the C_5 and C_6 fractions are poorly separated (Figure 5a). In the C_6 fraction the desired separation of hexane, monobranched and dibranched isomers is limited. Among the C_6 isomers, the highest partition coefficient amounts to 1.18 (for 2,3-dimethylbutane with respect to hexane). Adsorption enthalpy and entropy were estimated from the temperature dependence of retention times using van't Hoff plots (Figure 5a,b, insert). Adsorption enthalpies of the alkanes on the COK-18 and HKUST-1 are in the desired range of low values (see Table 1 and Table S9). The adsorption enthalpy of the C_6 alkanes on COK-18 e.g. is below 51 kJ mol^{-1} (*n*-hexane, $-\Delta H$ = 50.3 kJ mol^{-1}). These values are similar to the adsorption enthalpy of ordered mesoporous silica materials such as the gyroid type MCM-48 and a microporous/mesoporous variant, Zeotile-2[58] and well below the typical values above 60 kJ mol^{-1} observed on zeolites.[35] Despite the indistinguishable adsorption enthalpies of COK-18, HKUST-1 and MCM-48, MCM-48 does not show any molecular shape selectivity on alkane separation.[58]

For HKUST-1 material, a substantial chromatographic peak broadening was observed which could be ascribed to intracrystalline mass transfer resistance (Figure 5a). Concerning diffusion and the advantage of the hierarchical pore system, there is a clear sharpening of the chromatographic peaks with COK-18 compared to HKUST-1. Although peaks width is dependent on many parameters, given the similarity of packing, the strong differences in micropore and mesopore size seems to contribute to a better mass transport in COK-18. The importance of mesopore networks in microporous materials for eliminating their transport limitations have been well-discussed by Valiullin and co-workers.[59-61] COK-18 has mesopore with calculated $V_{meso}/V_{particle}$ ratio of *ca.* 16%. The mesopores which empty in relative pressure range 0.4-0.5 (P/P_o) by cavitation are fairly large, but should be connected to much narrower micropores (*ca.* 1.1 nm in diameter) as evidenced from the N2 adsorption-desorption isotherm and electron tomography as shown in Figure 1b and Figure 1g, respectively. Despite the lower $V_{meso}/V_{particle}$ ratio,

Table 1. Values of enthalpy, entropy and free Gibbs adsorption energies and partition coefficients α_{hexane} of the studied alkanes obtained from the variable temperature pulse gas chromatographic studies using COK-18 as chromatographic bed. The free energy was calculated using $\Delta G = \Delta H_{iso} - T\Delta S$.

Studied alkanes	$-\Delta H_{diff}$ (kJ mol^{-1})	$-\Delta H_{iso}$ (kJ mol^{-1})	$-\Delta S$ (J K^{-1} mol^{-1})	$-\Delta G$ (kJ mol^{-1})	$\alpha_{hexane/x}$ (x)
propane	17.9	21.4	61.0	-3.84	14.9
butane	30.5	33.9	85.8	-1.52	7.78
pentane	37.4	40.9	96.0	1.21	3.44
2-methybutane	30.7	34.1	80.2	1.01	3.65
n-hexane	50.4	53.8	117.2	5.43	1.00
2-methylpentane	38.6	42.1	90.8	4.57	1.29
3-methylpentane	41.1	44.5	96.1	4.80	1.20
2,2-dimethylbutane	42.7	46.2	101.8	4.12	1.47
2,3-dimethylbutane	40.0	43.5	94.4	4.47	1.32

the much widened rhombic pore entrance of COK-18 (1.1 nm) versus a much narrower cubic pore entrance of HKUST-1 (0.9 nm) seen from the [100] direction is expected to facilitate the adsorption and diffusion of the hydrocarbon compounds.[62] As molecule adsorption and diffusion would take place predominantly within individual pore channels, the interchannel diffusion would be very much limited by the narrow pore window between adjacent channels. It should be mentioned that HKUST-1 has a bimodal pore size distribution. It consists of main channels of *ca.* 0.9 nm diameter and tetrahedral side pockets of *ca.* 0.5 nm, which are interconnected to the main channels by triangular pore windows of *ca.* 0.35 nm in diameter.[62] The presence of small pore window might be too tight for hexane isomers to pass through as clearly evidenced from peak broadening that ascribed to poor kinetics of diffusion of the alkanes over HKUST-1 (Figure 5b). The wide channels in combination with the unique chemistry of the 3D COK-18 structure containing the unsaturated sites of Cu(II) and nucleophilic hydroxyl units present on the pore walls are proposed to lead to notably different in mass transportation which are expected to facilitate mass transport to achieve the modest adsorption enthalpy and entropy necessary for a multicomponent molecular separation process at low temperature.[63-66]

Adsorption enthalpy differences are compensated by enthalpy difference leading overall to minor variation of Gibbs free energy of adsorption and small separation factors of HKUST-1 (Table S9). By contrast, COK-18 shows an improved performance in both aspects *viz.* in terms of separation and peak broadening (Figure 5b). The retention order of the alkanes is: methane < ethane < propane < butane < 2-methylbutane < pentane < 2,2-dimethylbutane < 2,3-dimethylbutane < 2-methylpentane < 3-methylpentane < *n*-hexane. COK-18 clearly enhanced the partition coefficients, which reached e.g. 1.47 for 2,2-

dimethylbutane with respect to *n*-hexane (see Table 1), compared to 1.15 on HKUST-1. The enhanced separation is due to significant adsorption entropy and enthalpy differences as shown in Table 1. Adsorption energy differences between linear and branched alkanes on COK-18 are substantial (Table 1). For instance, it amounts to 27 J K^{-1} mol^{-1} for *n*-hexane compared to 2-methylpentane. In the microporous/mesoporous hybrid silica material Zeotile-2 having similar adsorption enthalpies, the adsorption entropy difference is hardly more than 5 J K^{-1} mol^{-1}.[55]

In enthalpy driven separations, the high temperature needed for molecular mobility is detrimental to selectivity. For MOFs with a much narrower pore such as Al-fumarate (0.57 x 0.6 nm^2), gas chromatographic separation of 2,3-dimethylbutane, 3-methylpentane and *n*-hexane at 483 K,[46] resulted in a much higher adsorption enthalpy (–ΔH for 2,3-dimethylbutane 3-methylpentane and hexane of 56.8, 66.3 and 68.4 kJ mol^{-1}), only marginally different from zeolites. On the other hand, separation of hexane isomers over a MOF with much open pore structure (MIL-47) in the temperature range of 393-493 K revealed substantially lower adsorption enthalpies of 2-methylpentane, 2,2-dimethylbutane, 2,3-dimethylbutane and *n*-hexane corresponding to 47.7, 48.3, 48.5 and 50.6 kJ mol^{-1}, respectively. This confirms the expectation of lower adsorption enthalpy in a MOF with sufficiently wide pores.[47]

Alkane adsorption revealed very strong differences between COK-18 and HKUST-1. Especially the adsorption entropy differences between the alkanes are much more pronounced on COK-18 emphasizing the potential of entropy driven separation. Previous work on hexane isomer separation has been focused on kinetic effects.[40,44] The $Fe_2(BDP)_3$ material achieves nicely the separation of hexane isomers according to the number of branching, but does not separate positional isomers.[32] Long columns of porous organic cage (CC3-R) material are needed to separate the full mixture, while in the present work separation was obtained with a much shorter column.[67]

Molecular simulation. Grand canonical Monte Carlo (GCMC) simulation was performed to provide microscopic insight into alkane adsorption in COK-18. The simulation details are provided in the Methods. Figure 5c shows the adsorption isotherms of the experimentally studied 11-component mixture at 373 K. The adsorption capacity increases as methane < ethane < propane < butane < 2-methylbutane < pentane < 2,2-dimethylbutane < 2,3-dimethylbutane < 3-methylpentane < 2-methylpentane < *n*-hexane. This closely follows the trend of the experimentally determined gas chromatogram (Figure 5b) and emphasizes a high degree of selectivity towards *n*-hexane. This sequence is attributed to polarization and configurational entropy effects. For linear alkanes, the interaction with the framework becomes stronger when length (polarizability) increases. For the linear and branched isomers, however, the packing efficiency in the pores decreases with increasing degree of branching. The partition coefficients between *n*-hexane and other components at 1 bar were estimated and show close agreement with the experimental data. The snapshots shown in Figure 5d illustrate the density distributions of *n*-hexane molecules adsorbed in COK-18. At a low pressure (1 kPa), *n*-hexane molecules mostly populate site I with low occupation of site II. Because of its vicinity to the metal clusters, site I is a stronger adsorption site compared to site II. With increasing the pressure to 10 kPa, the densities at both sites increase, until at high pressure (100 kPa), both sites are nearly fully occupied. From these observations, it is evident that *n*-hexane isomers interact strongly with the incomplete copper paddlewheels in COK-18, in good agreement with the experimental results.

CONCLUSIONS

In summary, we demonstrate the synthesis of a hierarchical MOF COK-18 via thermo-induced 1D-2D-3D solid-solid transformation. As a proof of concept, we also show that widening the micropores and introducing hierarchical porosity in a MOF lead to an improved multicomponent hydrocarbon separation compared to conventional microporous HKUST-1 and hierarchical silicate based materials. The interconnected hierarchical pore system reduces the diffusion limitation and the low adsorption energies result in a thermodynamically controlled separation of a 11-hydrocarbon fractions in a single feed mixture. The entropy driven adsorption selectivity based on size and degree of hydrocarbon branching, next to the discovered solid-solid transformation mechanism will potentially inspire material design and open up a new direction of material synthesis, to achieve other important hydrocarbon separation processes such as olefin/paraffin separation to be performed at lower temperature.

EXPERIMENTAL SECTION

Synthesis of COK-18. CuBTC precursor material (H1 phase) was prepared by mixing two separate synthesis solutions of 0.8585 g (3.55 mmol) of $Cu(NO_3)_2{\cdot}3H_2O$ (99-104%, Sigma-Aldrich) dissolved in 8.3 mL of distilled water and 0.4007 g (1.91 mmol) of BTC (95%, Sigma-Aldrich) dissolved in 10 mL of absolute ethanol (BDH) under magnetic stirring for 1 h at room temperature. The suspension was then transferred into a Teflon-lined stainless steel autoclave and treated in a preheated oven at 383 K for 2 days. The solid was recovered by filtration, washed with water:ethanol mixture (1:1= v/v) and dried at 333 K. Elemental analysis of activated COK-18: Anal. Calcd. For $Cu_{20}C_{72}H_{40}O_{64}$: Cu, 39.72; C, 27.03. Found: Cu, 40.11; C, 28.40.

Characterization of COK-18. COK-18 was characterized by a scanning electron microscope (SEM, Philips XL-30 FEG equipped with a tungsten filament). Prior to imaging, the sample was gold sputtered. Nitrogen adsorption isotherms were recorded using Micromeritics Tristar 3000 and Autosorb-1 instrument (Quantachrome, USA) instruments at 77 K. The samples were evacuated at 423 K under N_2 flow or vacuum for 12 h. XRD patterns were collected using a powder X-ray diffractometer (XRD, STOE STADI MP diffractometer with a linear position

sensitive detector (PSD) (6° 2θ window) in the region 2θ = 3 to 90°, with a step width of 0.5°, internal PSD resolution 0.01°, and a steptime of 400 s. The measurements were performed in Debye-Scherrer mode at room temperature using CuKα1 radiation with λ = 1.54056 Å selected by means of a Ge(111) monochromator. TG analysis was performed using a thermogravimetric instrument (TGA, Q 500) under nitrogen flow at a heating rate of 3 °C min^{-1} until 1173 K.

BF TEM, SAED and electron tomography. Bright field transmission electron microscopy (BF TEM) and selected area electron diffraction (SAED) was carried out using a Philips CM 20 electron microscope, operated at 200 kV. High angle annular dark field scanning transmission electron microscopy (HAADF-STEM) and electron tomography was performed using a FEI Tecnai 2G electron microscope operated at 200 kV. For the tomography series acquisition the step size of 5° was used to tilt the particle in range of -60° to 70°. SIRT algorithm (30 iterations) was carried out using the FEI inspect 3D software, followed by the 3D visualization using the FEI AMIRA software package.

FTIR, FIR and ATR. Infrared spectra were performed on powders in the form of thin self-supporting pellets. The pellets were put in specifically designed cryogenic cell that allows both an *in-situ* high temperature activation under vacuum or in a controlled atmosphere and the collection of FTIR spectra at a fixed temperature and in presence of the desired equilibrium pressure of gaseous molecular probes. All samples were activated under vacuum conditions at 453 K for 2 hours. FTIR spectra relative to CO adsorption at 77 K were recorded in the mid-IR range on the activated samples in the absorbance mode, at 2 cm^{-1} resolution, on a Nicolet 6700 spectrophotometer equipped with a liquid N_2 cooled MCT detector. Far-IR spectra have been collected at a resolution of 4 cm^{-1} on a Bruker Vertex 70 instrument, equipped with a Si beam splitter and a far-IR DTGS detector. The samples have been diluted in paraffin. On the same instrument, mid-IR region spectra in ATR mode (Attenuated Total Reflectance) have been collected at a resolution of 4 cm^{-1} using a DTGS detector.

Variable temperature pulse chromatography. Gas-phase adsorption at zero coverage surface was studied using the pulse chromatographic technique employing a gas chromatograph and stainless steel 15 cm-column (0.4 cm internal diameter) packed with *ca.* 0.7 g of the studied materials (COK-18 and HKUST-1). Prior to measurement, samples were activated overnight at 443 K in a He flow (20 mL min^{-1}). The samples were reactivated after each pulse gas experiment and each measurement was repeated for at least three times. The structure of COK-18 remains intact after sequential activation-reactivation cycles. Later on, a complex gas mixture composed of C_1-C_4 gases (0.4 mL) and liquid phase of C_5-C_6 (4 μL) was injected at 1 bar and the separation performance of the chromatographic column was examined at variable temperatures (403-433 K) by means of a mass spectrometer gas analysis system (Pfeiffer Vacoon), detecting the corresponding masses. The different isomers were injected separately in order to accurately determine their retention time. The dead volume of the system was calculated using the retention time of hydrogen as a reference. The zero-coverage thermodynamic parameters of the adsorption process were calculated using a van't Hoff type analysis employing isothermal chromatographic measurements (Münch and Florian O. R. L. Mertens). The retention volumes were corrected taking into account the volume expansion of the gas entering the capillary due to the temperature increase according to $V_N = (t_R - t_m)F_a(T/T_a)j$ where V_N = net retention volume (ml); t_R = retention time (min); t_m = dead time (min); F_a = volumetric flow-rate measures at ambient temperature (ml min^{-1}); T= column temperature (K); T_a = ambient temperature (K); the James–Martin gas compressibility correction $j = (3(p_i/p_o)^2-1)/(2(p_i/p_o)^3-1)$ where p_i = pressure of gas applied to the chromatogram and P_o = pressure of gas at outlet.

Once these correction where applied, the van't Hoff plot of the equation $\ln V_N = \ln(RTn_s) + \Delta S/R - \Delta H_{diff}/(RT')$ was used to calculate the thermodynamic parameters of each analyte taking into account the term $\ln(RTn_s)$ is usually small and can be neglected in the determination of ΔS. In addition to the ΔH_{diff} value obtained from the van't Hoff plot the isosteric heat of adsorption (ΔH_{iso}) was also determined according to the relation $|\Delta H_{iso}| = |\Delta H_{diff}| + RT_{average}$. The $\alpha_{alkane/hexane}$ partition coefficients have been calculated from the ratio of V_N for each gas at 423 K.

Molecular simulation. Grand canonical Monte Carlo (GCMC) method was adopted to simulate the adsorption of 11-component mixture in COK-18 at 373 K. The experimentally determined crystallographic data served as a structure model for COK-18. The disperse interactions of COK-18 were mimicked by the universal force field (UFF).[68] A number of simulation studies have shown that UFF can accurately predict gas adsorption in various MOFs.[69,70] The alkanes were described by the TraPPE force field,[71,72] and the interactions between COK-18 and alkanes were estimate by the Lorentz-Berthelot combining rules. The framework of COK-18 was assumed to be rigid and the periodic boundary conditions were used in three dimensions. As adsorption is usually focused on low-energy equilibrium configurations, the incorporation of framework flexibility would not exert a significant effect. The mixture consisted of equimolar methane, ethane, propane, butane, pentane, hexane, 2-methylbutane, 2,2-dimethylbutane, 2,3-dimethylbutane, 2-methylpentane and 3-methylpentane. The Peng-Robinson equation of state was used to convert fugacities into pressures. To sample long alkanes, the conventional Metropolis technique is prohibitively expensive. Instead, the advanced configurational-bias technique was used here to improve sampling efficiency,[73] in which a molecule was grown atom-by-atom biasing energetically favorable configurations while avoiding overlap with other atoms. Firstly, ten trial positions were generated with a probability proportional to:

$\exp(-\beta U^{i}_{\text{internal}})$, where $\beta = 1/k_B T$ and U^{i}_{internal} is the internal energy at a position *i* including the intramolecular bond bending and dihedral torsion interactions. Then, one of the trial positions was chosen for growing an atom with a probability proportional to: $\exp(-\beta U^{i}_{\text{external}}) / \sum_i \exp(-\beta U^{i}_{\text{external}})$, where U^{i}_{external} is the external energy including all non-bonded intramolecular and intermolecular interactions. Furthermore, the insertion of molecules was enhanced using the multiple first-bead scheme with ten trial positions.[74] A spherical cut off length equal to half of the minimum box length was used to evaluate the disperse interactions with long-range corrections included. A typical GCMC simulation was carried out for 2×10^6 cycles, in which the first 10^6 cycles were used for equilibration and the second 10^6 cycles for ensemble averages. Each cycle consisted of different types of trial moves: (a) translation. A randomly selected adsorbate molecule was translated with a random displacement in either x, y or z dimension, and the maximum displacement was adjusted to an overall acceptance ratio of 50%. (b) rotation. A randomly selected adsorbate molecule was rotated around either x, y or z dimension with a random angle, and the maximum angle was adjusted to an overall acceptance ratio of 50%. (c) partial regrowth. Part of a randomly selected adsorbate molecule was regrown locally. It was decided randomly which part of the molecule was regrown and from which bead the regrowth was started. (d) complete regrowth. A randomly selected adsorbate molecule was regrown completely at a random position. (e) swap with reservoir. A new adsorbate molecule was created at a random position, or a randomly selected adsorbate molecule was deleted. To ensure microscopic reversibility, the creation and deletion were attempted at random with equal probability. (f) exchange of molecular identity. An alkane molecule was selected randomly and an attempt was made to change its molecular identity. All the simulations were performed using the RASPA package.[75]

ASSOCIATED CONTENT

The supporting information is available free of charge via the Internet at http://pubs.acs.org. DFT pore size distribution of COK-18, TGA profile of COK-18, mid-IR spectra of activated COK-18, HKUST-1 and dense H1 precursor, mid-IR spectra in ATR mode of COK-18, HKUST-1 and dense H1 precursor, FTIR spectra in the increasing coverages of CO on COK-18 and HKUST-1, physicochemical properties of COK-18 samples recovered at different solvothermal synthesis time, rietveld refinement, listing of lattice parametres (refined) and atomic coordinates of H3, H6, H9, H12, COK-18 as made and COK-18 activated, reliability factor and phase content of COK-18 at different synthesis times, values of enthalpy, entropy and free Gibbs adsorption energies and partition coefficients of the studied alkanes over HKUST-1 (PDF). X-ray crystallographic data for COK-18 (as-made) and COK-18 (activated) (CIF). Three-dimensional visualization of COK-18 hierarchical pore structure by electron tomography and solid-solid transformation scheme and folding mechanism of flattened hexagonal sheets into octahedra with striated pattern (Video).

AUTHOR INFORMATION

Corresponding Author

* likhong.wee@kuleuven.be
*chejj@nus.edu.sg
*jarn@ugr.es
*christine.kirschhock@kuleuven.be

Notes

The authors declare no competing financial interest.

ACKNOWLEDGMENT

L.H.W. and S.T. thank Research Foundation Flanders (FWO) for a postdoctoral research fellowship under contract number of 12M1415N and G004613N, respectively. J.J. is grateful to the National University of Singapore for financial supports (R261-508-001-646/733 and R-279-000-474-112). J.A.R.N. thanks generous funding from Spanish Ministry of Economy (CTQ2014-53486-R) and FEDER and Marie Curie IIF-625939 (L.M.R.A) funding from European Union. J.A.M. gratefully acknowledges financial supports from Flemish Government (Long-term structural funding Methusalem). Collaboration among universities was supported by the Belgian Government (IAP-PAI network). We thank E. Gobechiya for XRD measurements. We would like to acknowledge Dr. Matthias Thommes for the discussion on the interpretation of N2 physisorption isotherms.

REFERENCES

(1) Schoedel, A.; Li, M.; Li, D.; O'Keeffe, M.; Yaghi, O. M. *Chem. Rev.* **2016**, *116*, 12466.

(2) Zhou, H. -C.; Kitagawa, S. *Chem. Soc. Rev.* **2014**, *43*, 5415.

(3) Guillerm, V.; Kim, D.; Eubank, J. F.; Luebke, R.; Liu, X.; Adil, K.; Lah, M. S.; Eddaoudi, M. *Chem. Soc. Rev.* **2014**, *43*, 6141.

(4) Férey, G. *Chem. Soc. Rev.* **2008**, *37*, 191.

(5) Furukawa, H.; Cordova, K. E.; O'Keeffe; M. Yaghi, O. M. *Science* **2013**, *341*, 1230444.

(6) Li, M.; Li, D.; O'Keeffe, M.; Yaghi, O. M. *Chem. Rev.* **2014**, *114*, 1343.

(7) Ockwig, N. W.; Delgado-Friedrichs, O.; O'Keeffe, M.; Yaghi, O. M. *Acc. Chem. Res.* **2005**, *38*, 176.

(8) Corma, A.; García, H.; Llabrés i Xamena, F. X.; *Chem. Rev.* **2010**, *110*, 4606.

(9) Jiang, J.; Yaghi, O. M. *Chem. Rev.* **2015**, *115*, 6966.

(10) Murray, L. J.; Dincă, M.; Long, J. R. *Chem. Soc. Rev.* **2009**, *38*, 1294.

(11) Suh, M. P.; Park, H. J.; Prasad, T. K.; Lim, D. -W. *Chem. Rev.* **2012**, *112*, 782.

(12) Farha, O. K.; Yazaydın, A. Ö.; Eryazici, I.; Malliakas, C. D.; Hauser, B. G.; Kanatzidis, M. G.; Nguyen, S. T.; Snurr, R. Q.; Hupp, J. T. *Nature Chem.* **2010**, *2*, 944.

(13) He, Y.; Zhou, W.; Qian, G.; Chen, B. *Chem. Soc. Rev.* **2014**, *43*, 5657.

(14) Li, J. -R.; Kuppler, R. J.; Zhou, H. -C. *Chem. Soc. Rev.* **2009**, *38*, 1477.

(15) Kreno, L. E.; Leong, K.; Farha, O. K.; Allendorf, M.; Van Duyne, R. P.; Hupp, J. T. *Chem. Rev.* **2012**, *112*, 1105.

(16) Horcajada, P.; Chalati, T.; Serre, C.; Gillet, B.; Sebrie, C.; Baati, T.; Eubank, J. F.; Heurtaux, D.; Clayette, P.; Kreuz, C.; Chang, J. -S.; Hwang, Y. K.; Marsaud, V.; Bories, P. -N.; Cynober, L.; Gil, S.; Férey, G.; Couvreur, P.; Gref, R. *Nature Mater.* **2010**, *9*, 172.

(17) Yue, Y.; Fulvio, P. F.; Dai, S. *Acc. Chem. Res.* **2015**, *48*, 3044–3052

(18) Reboul, J.; Furukawa, S.; Horike, N.; Tsotsalas, M.; Hirai, K.; Uehara, H.; Kondo, M.; Louvain, N.; Sakata, O.; Kitagawa, S. *Nature Mater.* **2012**, *11*, 717.

(19) Férey, G.; Mellot-Draznieks, C.; Serre, C.; Millange, F.; Dutour, J.; Surblé, S.; Margiolaki, I. *Science* **2005**, *309*, 2040.

(20) Eddaoudi, M.; Kim, J.; Rosi, N.; Vodak, D.; Wachter, J.; O'Keeffe, M.; Yaghi, O. M. *Science* **2002**, *295*, 469.

(21) Wang, B.; Côté, A. P.; Furukawa, H.; O'Keeffe, M.; Yaghi, O. M. *Nature* **2008**, *453*, 207.

(22) Deng, H.; Grunder, S.; Cordova, K. E.; Valente, C.; Furukawa, H.; Hmadeh, M.; Gándara, F.; Whalley, A. C.; Liu, Z.; Asahina, S.; Kazumori, H.; O'Keeffe, M.; Terasaki, O.; Stoddart, J. F.; Yaghi, O. M. *Science* **2012**, *336*, 1018.

(23) Koh, K.; Wong-Foy, A. G.; Matzger, A. J. *Angew. Chem. Int. Ed.* **2008**, *47*, 677.

(24) Chevreau, H.; Devic, T.; Salles, F.; Maurin, G.; Stock, N.; Serre, C. *Chem. Int. Ed.* **2013**, 52, 5056.

(25) Bradshaw, D.; El-Hankari, S.; Lupica-Spagnolo, L. *Chem. Soc. Rev.* **2014**, *43*, 5431.

(26) Wee, L. H.; Wiktor, C.; Turner, S.; Vanderlinden, W.; Janssens, N.; Bajpe, S. R.; Houthoofd, K.; Van Tendeloo, G.; De Feyter, S.; Kirschhock, C. E. A.; Martens, J. A. *J. Am. Chem. Soc.* **2012**, *134*, 10911.

(27) Wee, L. H.; Lescouet, T.; Ethiraj, J.; Bonino, F.; Vidruk, R.; Garrier, E.; Packet, D.; Bordiga, S.; Farrusseng, D.; Herskowitz, M.; Martens, J. A. *ChemCatChem* **2013**, *5*, 3562.

(28) Peng, L.; Zhang, J.; Xue, Z.; Han, B.; Sang, X.; Liu, C.; Yang, G. *Nature Commun.* **2014**, *5*, 4465.

(29) Pham, M. -H.; Vuong, G. -T.; Fontaine, F. -G.; Do, T. -O. *Cryst. Growth Des.* **2012**, *12*, 1008.

(30) Yaghi, O. M. *Nat. Mater.* **2007**, 6, 92.

(31) Shekhah, O.; Wang, H.; Paradinas, M.; Ocal, C.; Schüpbach, B.; Terfort, A.; Zacher, D.; Fischer, R. A.; Wöll., C. *Nature Mater.* **2009**, *8*, 481.

(32) Herm, Z. R.; Wiers, B. M.; Mason, J. A.; van Baten, J. M.; Hudson, M. R.; Zajdel, P.; Brown, C. M.; Masciocchi, N.; Krishna R.; Long, J. R. *Science* **2013**, *340*, 960.

(33) Bárcia, P. S.; Silva, J. A. C.; Rodrigues, A. E. *Micropor. Mesopor. Mater.* **2005**, *79*, 145.

(34) Bárcia, P. S.; Silva, J. A. C.; Rodrigues, A. E. *Ind. Eng. Chem. Res.* **2006**, *45*, 4316.

(35) Bárcia, P. S.; Silva, J. A. C.; Rodrigues, A. E. *AIChE J.* **2007**, *53*, 1970.

(36) Krishna, R.; Smit, B.; Calero, S. *Chem. Soc. Rev.* **2002**, *31*, 185.

(37) Herm, Z. R.; Bloch, E. D.; Long, J. R. *Chem. Mater.* **2014**, *26*, 323.

(38) He, Y.; Krishna, R.; Chen, B. *Energy Environ. Sci.* **2012**, 5, 9107.

(39) Chen, B.; Liang, C.; Yang, J.; Contreras, D. S.; Clancy, Y. L.; Lobkovsky, E. B.; Yaghi, O. M.; Dai, S. *Angew. Chem.* **2006**, *118*, 1418.

(40) Mendes, P. A. P.; Horcajada, P.; Rives, S.; Ren, H.; Rodrigues, A. E.; Devic, T.; Magnier, E.; Trens, P.; Jobic, H.; Ollivier, J.; Maurin, G.; Serre C.; Silva, J. A. C. *Adv. Funct. Mater.* **2014**, *24*, 7666.

(41) Bárciaa, P. S.; Guimarães, D.; Mendes, P. A. P.; Silva, J. A. C.; Guillerm, V.; Chevreau, H.; Serre, C.; Rodrigue, A. E. *Micropor. Mesopor. Mater.* **2011**, *139*, 67.

(42) Chang, N.; Gu, Z. -Y.; Yan, X. -P. *J. Am. Chem. Soc.* **2010**, *132*, 13645.

(43) Dubbeldam, D.; Galvin, C. J.; Walton, K. S.; Ellis, D. E.; Snurr, R. Q. *J. Am. Chem. Soc.* **2008**, *130*, 10884.

(44) Bárcia, P. S.; Zapata, F.; Silva, J. A.; Rodrigues, A. E.; Chen, B. *J. Phys. Chem. B* **2007**, *111*, 6101.

(44) Chang, N.; Gu, -Z. -Y.; Wang, -H. -F.; Yan, -X. -P. *Anal. Chem.* **2011**, *83*, 7094.

(46) Bozbiyik, B.; Lannoeye, J.; Devos, D. E.; Boron, G. V.; Denayer, J. F. M. *Phys. Chem. Chem. Phys.* **2016**, *18*, 3294.

(47) Finsy, V.; Calero, S.; García-Pérez, E.; Merkling, P. J.; Vedts, G.; De Vos, D. E.; Baron, G. V.; Denayer, J. F. M. *Phys. Chem. Chem. Phys.* **2009**, *11*, 3515.

(48) Fan, L.; Yan, -X. -P. *Talanta* **2012**, *99*, 944.

(49) Pech, R.; Pickardt, J. Acta Crystallogr., Sect. C: Cryst. Struct. Commun. **1988**, *44*, 992.

(50) Sing, K. S. W.; Everett, D. H.; Haul, R. A. W.; Moscou, L.; Pierotti, R. A.; Rouquérol, J.; Siemieniewska, T. *Pure & Appl. Chem.* **1985**, *57*, 603.

(51) Kruk, M.; Jaroniec, M. *Chem. Mater.* **2001**, *13*, 3169.

(52) Chui, S. S.-Y.; Lo, S. M.-F.; Charmant, J. P. H.; Orpen, A. G.; Williams, I. D. *Science* **1999**, *283*, 1148.

(53) Prestipino, C.; Regli, L.; Vitillo, J. G.; Bonino, F.; Damin, A.; Lamberti, C.; Zecchina, A.; Solari, P. L.; Kongshaug, K. O.; Bordiga, S. *Chem. Mater.* **2006**, *18*, 1337.

(55) Hadjiivanov, K.; Knözinger, H. *J. Catal.* **2000**, *191*, 480.

(55) Bordiga, S.; Regli, L.; Bonino, F.; Groppo, E.; Lamberti, C.; Xiao, B.; Wheatley, P. S.; Morris, R. E.; Zecchina, A. *Phys. Chem. Chem. Phys.* **2007**, *9*, 2676.

(56) Drenchev, N.; Ivanova, E.; Mihaylova, M.; Hadjiivanov, K. *Phys. Chem. Chem. Phys.* **2010**, *12*, 6423.

(57) Katsenis, A. D.; Puškarić, A.; Štrukil, V.; Mottillo, C.; Julien, P. A.; Užarević, K.; Pham, M. -H.; Do, T. -O.; Kimber, S. A. J.; Lazić, P.; Magdysyuk, O.; Dinnebier, R. E.; Halasz, I.; Friščić, T. *Nature Commun.* **2015**, *6*, 1.

(58) Devriese, L. I.; Cools, L.; Aerts, A.; Martens, J. A.; Baron, G. V.; Denayer, J. F. M. *Adv. Funct. Mater.* **2007**, *17*, 3911.

(59) Schneider, D.; Mehlhorn, D.; Zeigermann, P.; Kärger, J.; Valiullin, R. *Chem. Soc. Rev.* **2016**, *45*, 3439.

(60) Zeigermann, P.; Naumov, S.; Mascotto, S.; J. Kärger, J.; Smarsly, B. M., Valiullin, R. *Langmuir* **2012**, *28*, 3621.

(61) Valiullin, R.; Naumov, S.; Galvosas, P.; Kärger, J.; Woo, H.-J.; Porcheron, F.; Monson, P. A. *Nature* **2006**, *443*, 965.

(62) Vishnyakov, A.; Ravikovitch, P. I.; Neimark, A. V.; Bülow, M.; Wang, Q. M. *Nano Lett.* **2003**, *3*, 713.

(63) Bao, Z.; Chang, G.; Xing, H.; Krishna, R.; Ren, Q.; Chen, B. *Energy Environ. Sci.* **2016**, *9*, 3612.

(64) Yang, S.; Ramirez-Cuesta, A. J.; Newby, R.; Garcia-Sakai, V.; Manuel, P.; Callear, S. K.; Campbell, S. I.; Tang, C. C.; Schröder, M.; *Nature Chem.* **2015**, *7*, 121.

(65) Llewellyn, P. L.; Horcajada, P.; Maurin, G.; Devic, T.; Rosenbach, N.; Bourrelly, S.; Serre, C.; Vincent, D.; Loera-Serna, S.; Filinchuk, Y.; Férey, G. *J. Am. Chem. Soc.* **2009**, *131*, 13002.

(66) Münch, A. S.; Mertens, F. O. R. L. *J. Mater. Chem.* **2012**, *22*, 10228.

(67) Kewley, A.; Stephenson, A.; Chen, L.; Briggs, M. E.; Hasell, T.; Cooper, A. I. *Chem. Mater.* **2015**, *27*, 3207.

(68) Rappe, A. K.; Casewit, C. J.; Colwell, K. S.; Goddard, W. A.; Skiff, W. M. *J. Am. Chem. Soc.* **1992**, *114*, 10024.

(69) Babarao, R.; Hu, Z. Q.; Jiang, J. W.; Chempath, S.; Sandler, S. I. *Langmuir* **2007**, *23*, 659.

(70) Zhang, K.; Chen, Y. F.; Nalaparaju, A.; Jiang, J. W. *CrystEngComm* **2013**, *15*, 10358.

(71) Martin, M. G.; Siepmann, J. I. *J. Phys. Chem. B* **1998**, *102*, 2569.

(72) Martin, M. G.; Siepmann, J. I. *J. Phys. Chem. B* **1999**, *103*, 4508.

(73) Siepmann, J. I.; Frenkel, D. *Mol. Phys.* 1992, **75**, 59.

(74) Esselink, K.; Loyens, L. D. J. C.; Smit, B. *Phys. Rev. E* **1995**, *51*, 1560.

(75) Dubbeldam, D.; Calero, S.; Ellis, D. E.; Snurr, R. Q. *Mol. Simul.* **2016**, *42*, 81.

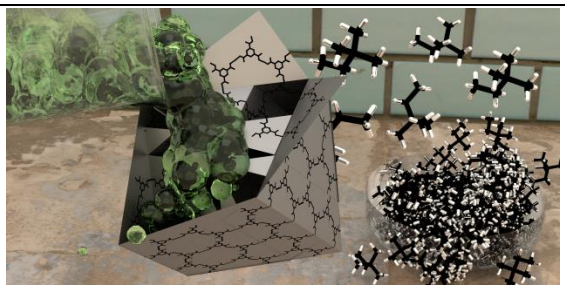

Table of Contents artwork